中国光学 Chinese Optics 核心期刊

Diverse surface waves supported by bianisotropic meta surfaces

YOU Ou-bo, GAO Wen-long, LIU Ya-chao, XIANG Yuan-jiang, ZHANG Shuang

Citation:
YOU Ou-bo, GAO Wen-long, LIU Ya-chao, XIANG Yuan-jiang, ZHANG Shuang. Diverse surface waves supported by bianisotropic meta surfaces[J]. *Chinese Optics*, 2021, 14(4): 782–791. doi: 10.37188/CO.2021–0098
游欧波, 高文龙, 刘亚超, 项元江, 张霜. 基于双各向异性超构表面的多样化表面波[J]. 中国光学, 2021, 14(4): 782–791. doi: 10.37188/CO.2021–0098

View online: https://doi.org/10.37188/CO.2021–0098

文章编号 2095-1531(2021)04-0782-10

Diverse surface waves supported by bianisotropic meta surfaces

YOU Ou-bo[1], GAO Wen-long[4], LIU Ya-chao[5], XIANG Yuan-jiang[3*], ZHANG Shuang[1,2*]

(1. *Department of Physics*, *The University of Hong Kong*, *Hong Kong China*;
2. *Department of Electrical & Electronic Engineering*, *The University of Hong Kong*, *Hong Kong China*;
3. *School of Physics and Electronics*, *Hunan University*, *Changsha* 410082, *China*;
4. *Department of Physics*, *Paderborn University*, *WarburgerStraße* 100, 33098 *Paderborn*, *Germany*;
5. *Institute of Microscale Optoelectronics*, *Shenzhen University*, *Shenzhen* 518060, *China*)

* *Corresponding author*, *E-mail*: *xiangyuanjiang*@126.*com*; *shuzhang@hku.hk*

Abstract: Surface waves supported by structured metallic surfaces, i.e.metasurfaces, have drawn wide attention recently.They are promising for various applications ranging from integrated photonic circuits to imaging and bio-sensing in various frequency regimes. In this work, we show that surface states with diverse polarization configurations can be supported by a metasurface consisting of a single layer of bianisotropic metamaterial elements.The structure possesses D_{2d} symmetry, which includes mirror symmetry in the *xz* and *yz* plane, and C_2 rotational symmetry along $y = \pm x$ axis. Due to this unique symmetry, the metasuface supports both transverse electric (TE) and transverse magnetic (TM) waves along k_x and k_y directions, while a purely longitudinal mode and an elliptically polarized transverse electromagnetic(TEM) mode along $k_y = \pm k_x$ directions. The versatility of the surface modes on the metasurface may lead to new surface wave phenomena and device applications.

Key words: surface plasmon; metasurface; bianisotropy; transverse electric; transverse magnetic

基于双各向异性超构表面的多样化表面波

游欧波[1], 高文龙[4], 刘亚超[5], 项元江[3*], 张 霜[1,2*]

(1. 香港大学物理學系, 香港, 中国;
2. 香港大学電機電子工程系, 香港, 中国;
3. 湖南大学物理与微电子科学学院, 长沙 中国, 410082;
4. Department of Physics, Paderborn University, Warburger Straße 100, Paderborn Germany, 33098;
5. 深圳大学微纳光电子学研究院, 深圳 中国, 518060)

摘要: 基于结构化的金属表面, 即超构表面, 所获得的表面波最近得到了广泛关注。它们在各种不同的频率下在集成光学回路、成像以及生物检测中都有着良好的应用前景。本文中, 我们展示了一种由双各向异性超构材料单元构成的超构表面可以支持多种不同偏振模式的表面态。这个结构拥有 D_{2d} 点群对称性, 包括了在 *xz* 和 *yz* 面内拥有镜面对称, 以及

收稿日期: 2021-05-01; **修订日期:** 2021-05-20

在 $y=\pm x$ 方向上拥有 C_2 旋转对称性。基于这种对称性，这个超构表面可以在 k_x 和 k_y 方向上支持横电模(TE)以及横磁模(TM)的同时支持在 $k_y=\pm k_x$ 方向上的纯纵模以及椭偏的横电磁模(TEM)。这种超构表面上的多种表面模式可能会产生新的表面波现象以及器件应用。

关　键　词: 表面等离子体激元; 超构表面; 双各向异性; 横电模; 横磁模
中图分类号: O43, TN201, TN25　　**文献标志码:** A　　**doi:** 10.37188/CO.2021-0098

1 Introduction

Surface plasmon polaritons (SPPs), due to their tight confinement to a metal/dielectric interface and large wave vectors, represent an important platform for various applications ranging from integrated photonic circuits to sensing applications[1-2]. However, at optical frequencies, due to the significant ohmic loss of metals, the applications of SPPs suffer from the short propagation lengths. At longer wavelengths, the loss of SPPs is significantly reduced at the cost of poor confinement of the SPPs in the dielectric material. In 2004, Pendry proposed the concept of spoof plasmon that could be supported by a corrugated metallic surface with an effective plasma frequency determined by the geometries of the metallic structures[3], which was subsequently experimentally verified[4]. This new scheme greatly improves the confinement of surface waves to the structured surfaces, and has attracted tremendous interests from the community of photonics. Various explorations have been carried out based on spoof plasmons, including rainbow slow light trapping effect[5-6], focusing of terahertz waves[7], terahertz subwavelength waveguides[8], and terahertz sensing[9].

Indeed, structured surfaces (or metasurfaces) can be engineered to provide more diverse functionalities that go beyond confinement of surface waves, such as wavefront and amplitude control[10-18], enhanced and tailored nonlinear optical processes[19-23], resulting in a wide range of applications including imaging, holography and bio-sensing[24-30]. These new functionabilities can arise from judicious engineering of the unit cells, benefitting from the unconventional electromagnetic responses of complex metamaterial designs such as artificial magnetism, hyperbolicity, chirality and bianisotropy[31-38]. Bianisotropy refers to a cross coupling between electric and magnetic responses along orthogonal directions. It can exist in structures that lack inversion symmetry but with preserved mirror symmetry. Bianisotropic metamaterials have shown some highly intriguing phenomena such as asymmetric absorption[39-40], optical spin-orbit coupling[41], and topological optical effects[42]. In the past decade, biansotropy has been employed for designing topological metamaterials, which have shown interesting phenomena such as Fermi arc states and transverse spin of bulk optical modes[43-46]. Compared to three dimensional bulk metamaterials, the ultrathin nature of bianisotropic metasurfaces could lead to more practical applications due to its low fabrication cost and highly compact physical sizes. In this work, we experimentally investigate the surface states supported by a bianisotropic metasurface and showcase a number of interesting effects – the existence of both TE and TM surface modes along certain directions[47], while helical transverse electromagnetic mode and longitudinal mode in some other directions.

2 Results and discussion

The configuration of the metasurface is illustrated in Fig. 1(a). Each unit cell of the metasurface consists of a saddle-shaped metallic loop. The same unit cell, when arranged in a three dimensional array, forms a type-I ideal Weyl metamaterial, as demonstrated previously[43]. Here we are interested in a metasurface consisting of a single layer of such structure, and therefore the bulk property is not well defined. Each unit cell can be considered as two perpendicular split ring resonators with opposite orientation of the openings. The structure possesses D_{2d} symmetry, which includes mirror symmetry in the

xz and *yz* plane, and C_2 rotational symmetry along $y = \pm x$ axis.The fundamental resonant mode of the unit cell is a combination of electrical dipole moment and magnetic dipole moment, each of which can be excited by both an electric field or a magnetic field oriented in the *x*–*y* plane.

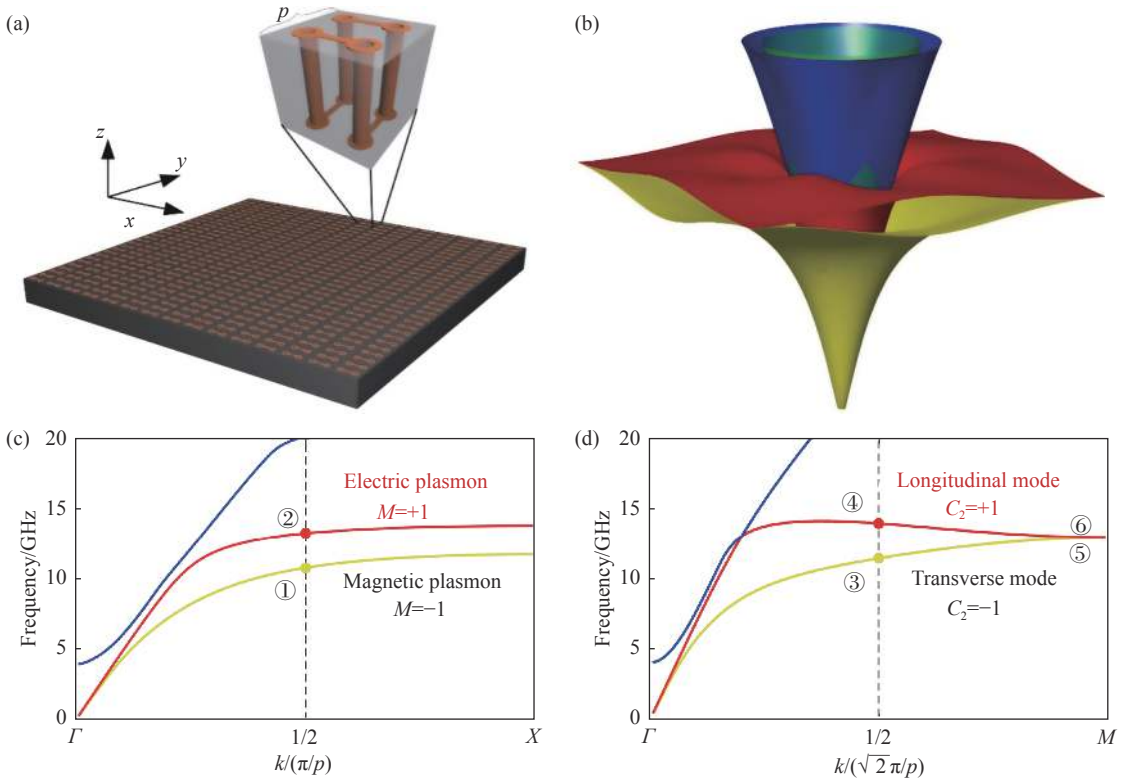

Fig. 1 (a) The schematic of the single-layer metasurface. Every unit cell consists of a saddle-shaped metallic inclusion possessing D_{2d} point symmetry embedded in the dielectric substrate whose relative permittivity is 2.2. The period of the metasurface along k_x or k_y is *p*. (b) The band structure of the metasurface. The 1st, 2nd, 3rd bands and light cone are plotted in yellow, red, blue and green, respectively. (c) The dispersions of the surface modes along k_y=0 direction. The modes along this direction corresponding to the 1st and 2nd bands can be regarded as electric plasmon and magnetic plasmon, respectively. (d) The dispersions of the surface modes along k_y=k_x direction. The modes along this direction for the 1st and 2nd bands can be regarded as transverse mode (elliptically polarized) and longitudinal mode, respectively

图 1 (a) 单层超构表面示意图。每一个单元都由在介电常数为 2.2 的基底中的拥有 D_{2d} 点群对称性的马鞍形金属内嵌物构成。该超构表面沿 k_x 或 k_y 方向的周期是 *p*; (b) 该表面的能带结构。第 1、2、3 条能带以及光锥分别由黄色、红色、蓝色以及绿色标出; (c) 该超构表面沿着 k_y=0 方向的色散。其中第 1、2 条能带在这个方向的模场分别是电等离子体激元以及磁等离子体激元; (d) 该超构表面沿着 k_y=k_x 方向的色散。其中第 1、2 条能带在这个方向的模场分别是横电磁模(椭偏)以及纵模

The band structure of the metasurface is shown in Fig. 1(b). There exist multiple bands in the system, with some bands located very close to the light cone (for example, the blue one). Here we are interested in the 1st and 2nd modes (yellow and red) with larger wave numbers. Due to the D_{2d} symmetry of the system, the wave propagation along *x* and *y* directions can be related to each other by simply a rotation of π about the k_x=±k_y axis. In order to have a clearer view of the dispersions of the surface waves, we plot the dispersions along the k_x/k_y direction in Fig. 1(c). The two lowest modes, labelled electric and magnetic plasmon in the figure, exhibit the typical surface plasmon dispersion features, i.e. an approximately linear dispersion at lower frequency, and the dispersion gradually become flat when approaching the effective plasma frequency[3]. We further plot the dispersions of the surface modes along

k_x=±k_y directions, as shown in Fig. 1(d). These 1st and 2nd modes are TEM and longitudinal modes, respectively.Interestingly, these two surface modes become degenerate at the corner of the Brillounin zone, i.e. **M** point. As will be explained later, this degeneracy arises from the D_{2d} symmetry of the system.

The existence of TE and TM modes can be analyzed through the point group symmetry. For modes along k_x/k_y direction, they must satisfy the mirror symmetry $M_{x/y}$ about *yz* or *xz* plane. The eigen values of M' are ±1. For M' = +1, the normal **E** field with respect to mirror plane will cancel out when integrated over the unit cell, while the parallel **E** field remains. Meanwhile, the **H** field, which is a pseudo vector field, behaves in the opposite way. Therefore this represents a TM mode. The M' = −1 mode, on the other hand, represents a TE mode based on a similar analysis. We further carry out full wave simulation, and present the field plots of the *x*-propagating modes in the *xz* cross-section plane cutting through the center of the unit cell in Fig. 2. For point ① on 1st mode in Fig. 1(c), the electric field is aligned along *y* direction, which is perpendicular to the propagation plane (Fig. 2(a)), whereas the magnetic field lies in the propagation plane having both *x* and *z* components (Fig. 2(b)). This confirms that 1st mode is not just a TE mode but also a magnetic surface plasmon mode, which is distinct from the conventional surface plasmon mode. It is interesting to note that the electric and magnetic field components are mostly confined to the top and bottom surfaces, respectively. On the other hand, the field distributions (Fig. 2(c) and 2(d)) of point ② on 2nd mode show opposite configuration as that of TE mode. Namely, the electric field lies in the propagation plane and the magnetic field is perpendicular to it, which represent the main features of conventional TM polarized surface plasmon modes. The presence of both TE and TM polarized surface plasmon modes can be attributed to the fact that the unit cell of the bianisotropic metasurface supports both electric and magnetic resonances.

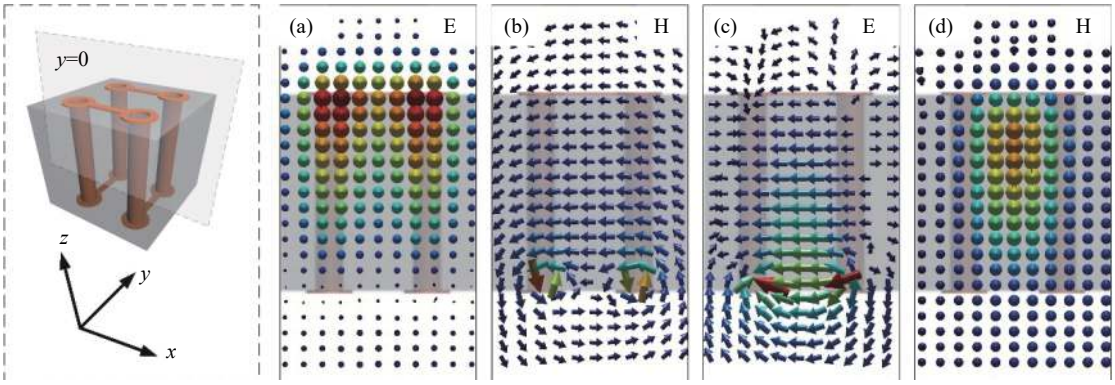

Fig. 2　Field distributions of surface plasmon modes propagating along *x* direction. On the left, the schematic of the unit cell illustrating the plane in which the fields are plotted is shown. (a, b) The E and H field distributions for point ① on 1st mode in Fig. 1(c). (c, d) The E and H fields for point ② on 2nd mode. k_x of point ① and ② is fixed at π/2*p*, where *p* is the period along *x* and *y* directions

图 2　沿着 *x* 方向传播的表面等离子体激元的场分布。场分布所在截面的位置在最左边的结构单元示意图中标出；(a, b) 在图 1(c) 中第 1 个模式上的点①处 E 和 H 分布；(c, d) 在图 1(c) 中第 2 个模式上的点②处 E 和 H 分布。点①和②处的 k_x 等于 π/2*p*, *p* 是沿 *x* 和 *y* 方向的结构周期

However, away from k_x/k_y directions, the surface plasmon modes are not exactly TE and TM modes anymore, but generally a hybridization between them. Interestingly, along k_x=±k_y directions, this hybridization leads to a complete re-arrangement of the field components, and the longitudinal mode and TEM mode emerge.The existence of the longitudinal mode and TEM can also be ana-

lyzed through the symmetry of the point group with respect to this direction. As the metasurface has C_2 symmetry along $k_x=\pm k_y$ directions, the eigen values of C_2 are ±1. For the $C_2 = +1$ mode, if we rotate the field by π about the symmetry axis, we will get the same field. This means that all the field components, both **E** and **H** perpendicular to the symmetry axis will cancel out when integrated over the unit cell, while fields components parallel to the symmetry axis remains, and therefore this corresponds to a longitudinal mode. For the $C_2 = -1$ mode, the situation is opposite, i.e. all longitudinal components cancel out while transverse components remain, which corresponds to a TEM mode. This is illustrated by the fields shown in Fig. 3. Fig. 3(a) and 3(b) show the distribution of the electric and magnetic fields of point ③ ($k_x=k_y=\pi/2p$) in Fig. 1(d), respectively, in a cross section plane perpendicular to the propagation direction. It is observed that both the **E** and **H** fields primarily lie in the plane, while the longitudinal components of the fields at different locations are opposite and cancel out, leading to an overall TEM mode. It is interesting to note that both the **E** and **H** fields rotate anticlockwise with time in the plane, i.e. the TEM mode is elliptically polarized. On the other hand, the distribution of **E** and **H** fields of point ④, as illustrated in Fig. 3(c) and 3(d) respectively, are primarily aligned along the propagation direction. Thus, it is confirmed that 1stmode is a pure longitudinal mode with both longitudinal **E** and longitudinal **H** components. We further look into the field distributions of the two points ⑤ and ⑥ in Fig. 1(d) close to **M** point in a horizontal plane (*xy* plane) cutting through the center of the unit cell, as shown by Fig. 3(e–h). The fields clearly show that the two modes can be related to each other through the following symmetry operations: a rotation of 90° in the *xy* plane about the center of the unit cell, followed by a mirror symmetry in *z* direction, which are consistent with the D_{2d} symmetry of the metasurface structure. Thus, this symmetry argument explains the degeneracy between the two modes at **M** point as shown in Fig. 1(d).

To measure the dispersion of the surface modes, we place a source antenna at the center of bottom surface of the sample, which consists of 90×70 unit cells, while the electric field distribution is mapped by a probe antenna raster-scanning the top surface. The Fourier transformations of the electric field, which represent the equal frequency contours (EFCs), at two representative frequencies of 10.9 GHz and 13.3 GHz are shown in Fig. 4(a) and 4(c), respectively, to illustrate the 1st and 2nd modes. The corresponding simulated results are shown in Fig. 4(b) and 4(d). The EFC of 1st band appears roughly as a round loop, as shown in Fig. 4(a, b). Inside the EFC of 1st band, the light cone and higher modes are crowded together into a bright smaller circle. The measured EFCs match well with the simulated ones shown in Fig. 4(b). At a higher frequency of 13.3 GHz, the EFC of 2nd band shows a more complicated pattern − an ellipse centered at the **Γ** point and four nearly straight lines close to the corner (Fig. 4(c)). Considering the periodic boundary of the Brilloun zone, these four lines indeed form a closed contour around the **M** point. The measured EFC agrees well with the simulation result (Fig. 4(d)), except for the missing of half of the elliptical contour with long axis oriented along *x* direction. This is because in the experiment only the top surface is measured, whereas the mode corresponding to the missing contour is mainly localized at the bottom surface. From the measured EFCs at different frequencies, one can retrieve the dispersion curves along different directions. As shown in Fig. 4(e), the experimentally retrieved dispersion of 1st and 2nd bands along k_x/k_y directions clearly show the characteristics of typical surface plasmons and they correspond to the TE and TM surface plasmon modes with different effective electric and magnetic plasma frequencies. However, along $k_x=\pm k_y$ directions, the two bands show very distinct features – while mode 1 shows similar dispersion as a conventional surface plasmon, mode 2 exhibits a negative

dispersion at large wavevectors (Fig. 4(f)). They become degenerate at **M** point, matching very well with the numerical results as indicated by the dashed lines.

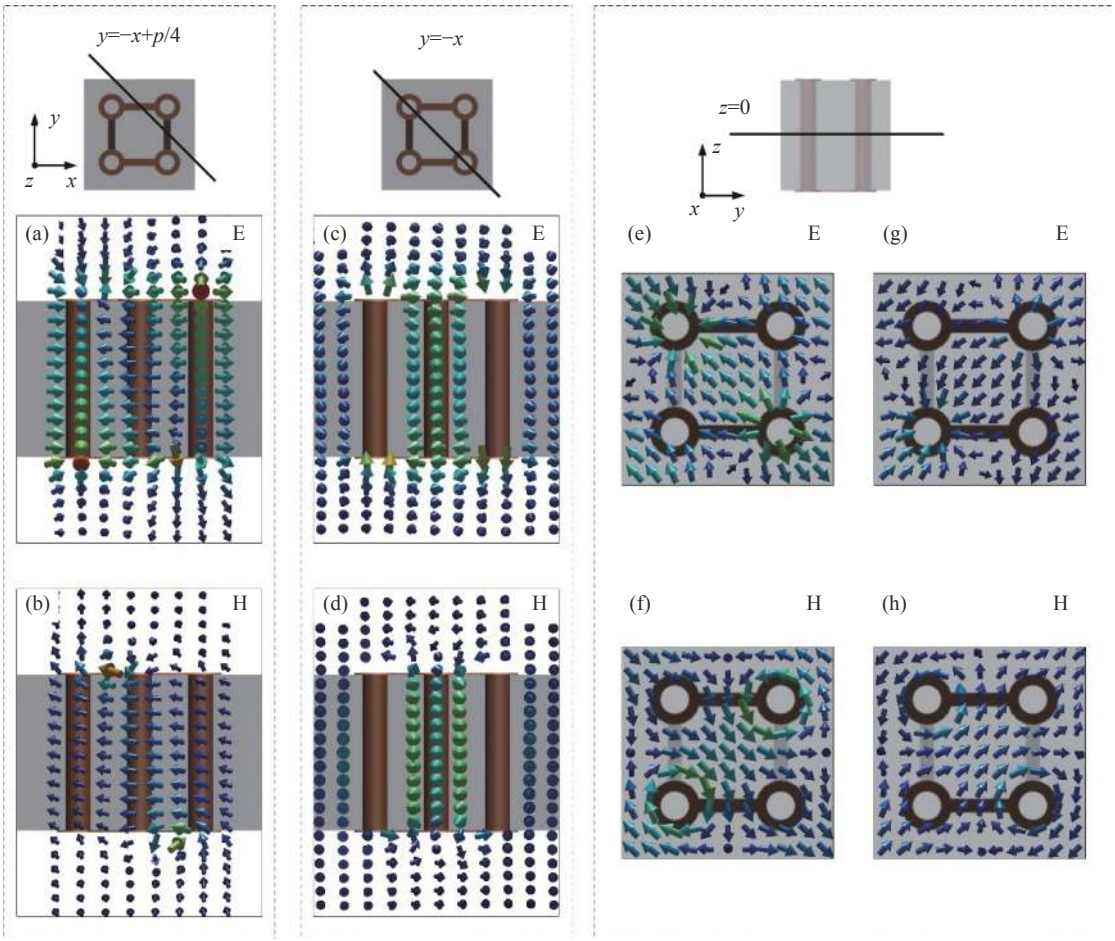

Fig. 3　Field distributions of surface plasmon modes propagating along k_x=k_y direction. (a, b) Field distributions of 1st mode at point ③ (k_x=k_y = π/2p) in Fig. 1(d). The simulated E (a) and H (b) field distributions in the plane perpendicular to the propagation direction, corresponding to the cutting plane shown in the schematic above. In both plots, the overall field distribution lie in the plane, indicating that this is a TEM mode. (c, d) Field distributions of 2nd mode at point ④ (k_x=k_y = π/2p) in Fig. 1(d). The simulated E (c) and H (d) field distributions in the plane perpendicular to the propagation direction, corresponding to the cutting plane shown in the schematic above. In both plots, the overall field distributions are out of plane (along the propagation direction), indicating that this is a pure longitudinal mode with both longitudinal components of E and H fields. (e-h) Field distributions of points ⑤ and ⑥ in Fig. 1(d), closing to the **M** point (phase advance is 170°), for a horizontal *xy* plane cutting through the center of the unit cell, as indicated by the schematic above. (e, f) correspond to the E and H field distributions of point ⑤, and (g, h) correspond to E and H field distributions of point ⑥. It is observed that the two modes are related to each other through an in-plane rotation of 90° about the center of the unit cell, followed by a mirror symmetry in *z* direction

图 3　沿 k_x=k_y 方向的表面等离子体激元模式的场分布。(a, b) 图 1(d) 中第 1 个模式在点③处 (k_x=k_y = π/2p) 的场分布。仿真得到的在垂直传播方向的面上的 **E** (a) 和 **H** (b) 场分布, 截面位置显示在上方示意图中。在两个图中, 总体的场分布都在面内, 证明了这是一个横电磁模。(c, d) 图 1(d) 中第 2 个模式在点④处 (k_x=k_y = π/2p) 的场分布。仿真得到的在垂直传播方向的面上的 **E** (c) 和 **H** (d) 场分布, 截面位置显示在上方示意图中。在两个图中, 总体的场分布都指向面外(沿着传播方向), 证明了这是一个同时拥有电场和磁场的纵模。(e-h) 图 1(d) 中非常接近 **M** 点的⑤和⑥处的穿过结构单元中心的 *xy* 截面处的场分布, (e, f) 分别代表了点⑤处的 **E** 和 **H** 场分布; (g, h) 分别代表了点⑥处的 **E** 和 **H** 场分布。通过一个面内关于结构单元中心的 90°旋转以及 *z* 方向上的镜面对称操作, 这两个模式之间可以进行互相转换

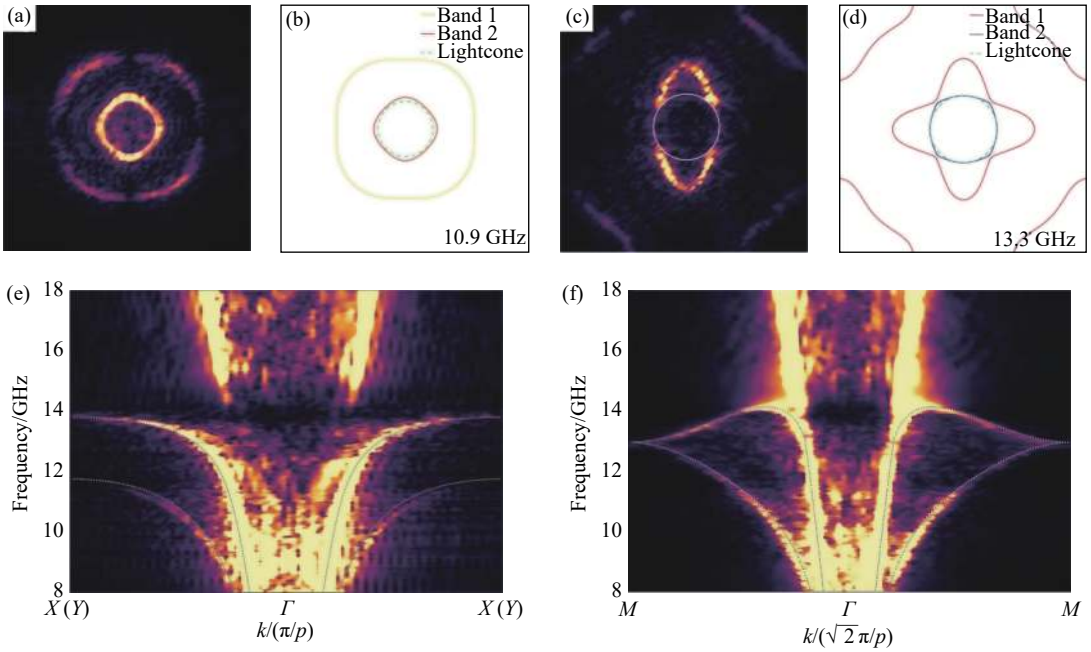

Fig. 4 Measured EFC and dipersion curves of the surface modes. The measured (a) and simulated (b) EFC at frequency of 10.9 GHz. The measured (c) and simulated (d) EFC at frequency of 13.3 GHz. (e, f) The dispersion of the surface modes along k_x/k_y and $k_x=\pm k_y$ directions, respectively. The dashed lines in the plots correspond to the simulation results

图 4 测量得到的表面模式的等频面以及色散曲线。测量 (a) 以及仿真 (b) 得到的在 10.9 GHz 处的等频面。测量 (c) 以及仿真 (d) 得到的在 13.3 GHz 处的等频面。(e, f) 表面模式沿着 k_x/k_y 和 $k_x=\pm k_y$ 方向上的色散曲线，虚线代表仿真结果

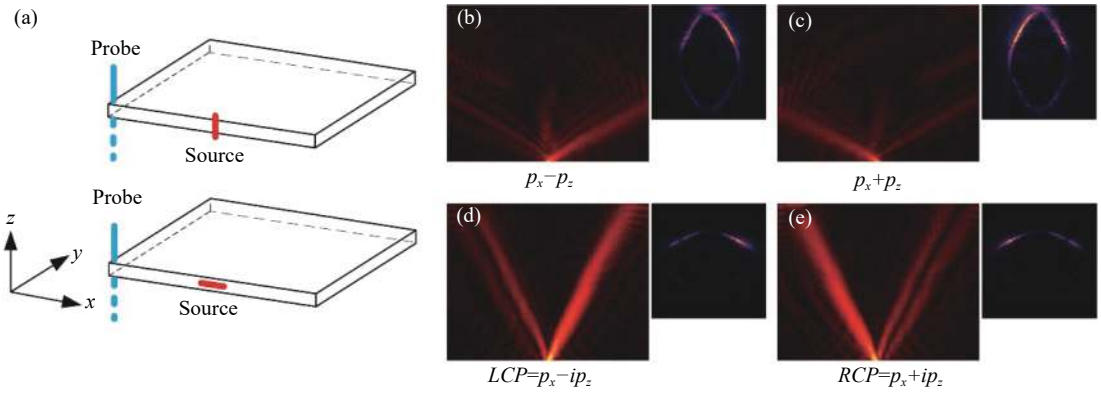

Fig. 5 Measurement of polarization controllable excitation of surface modes. (a) The experimental setup for measuring the surface mode. The excitation dipole antenna is oriented either in the vertical direction (upper panel) or the horizontal direction (lower panel). (b, c) Electric field distribution on top surfaces under polarization of p_x-p_z and p_x+p_z, respectively. (d, e) Same as (b, c) but the fields are measured on bottom surfaces under LCP and RCP excitation, respectively. All subplots attached to (b-e) are the corresponding EFCs in the Brillouin zone

图 5 入射偏振依赖的表面模式激发的实验结果。(a) 测量表面模式的实验设置。激发偶极天线的摆放方向或者垂直(上方示意图)或者水平(下方示意图)；(b, c) 上表面在 p_x-p_z 或 p_x+p_z 激发下的电场分布。(d, e) 下表面在 LCP 或 RCP 激发下的电场分布。(b~e) 所有的子图都代表了布里渊区等频面

Finally we experimentally investigate the excitation of the surface waves by controlling the orientation of the source dipole antenna. The experimental setup for the measurement is shown in Fig. 5(a). A source antenna is oriented along either x or z direction in the middle of the edge along x direction. For both configurations, we measure the field distributions on either the top surface or the bottom surface of the metasurface. By combining the two measured field distributions with source dipole an-

tenna oriented along the two orthogonal directions (x and z), one can retrieve the field distribution for tilted dipole antenna (e.g.orientation of +45° and −45°) and for circularly polarized antenna (left and right handed). Fig. 5(b) and 5(c) show the field patterns excited by a dipole antenna oriented along +45° and −45°, respectively, wherein the surface wave primarily propagates towards the left or the right hand side depending on the polarization of the exciting antenna. The field distributions also show very distinct features on the two sides when the source antenna is circularly polarized-a single beam appearing on one side and two split beams appearing on the other side, as shown by Fig. 5(d) and 5(e). The configurations are swapped when the rotating direction of the source antenna is flipped. This directly demonstrates the spin and orientation controlled excitation of the surface waves on the metasurface. In this experiment, the excitation efficiency is not very high, but sufficient to see all exotic features of this metasurface. For achieving a higher excitation efficiency, the size and orientation of the antenna would require very fine adjustment to match the polarization of the mode.

3 Summary

In summary, we have designed and demonstrated a bianisotropic metasurface with a unique symmetry configuration and investigated the rich features of surface waves supported by the metasurface. We have shown that both TE and TM surface plasmon waves can exist along certain directions, while along some other directions, there exist a pure longitudinal mode with both electric and magnetic components, and an elliptically polarized transverse electromagnetic mode. Such diverse dispersion and polarization configurations of the surface plasmon modes provide new degrees of freedom for constructing compact photonic integrated devices.

This project was funded by the Research Grants Council of Hong Kong (AoE/P-502/20).

References:

[1] ZAYATS A V, SMOLYANINOV I I, MARADUDIN A A. Nano-optics of surface plasmon polaritons[J]. *Physics Reports*, 2005, 408(3-4): 131-314.

[2] BARNES W L, DEREUX A, EBBESEN T W. Surface plasmon subwavelength optics[J]. *Nature*, 2003, 424(6950): 824-830.

[3] PENDRY J B, MARTIN-MORENO L, GARCIA-VIDAL F J. Mimicking surface plasmons with structured surfaces[J]. *Science*, 2004, 305(5685): 847-848.

[4] HIBBINS A P, EVANS B R, SAMBLES J R. Experimental verification of designer surface plasmons[J]. *Science*, 2005, 308(5722): 670-672.

[5] GAN Q Q, FU ZH, DING Y J, *et al*.. Ultrawide-band width slow-light system based on THz plasmonic graded metallic grating structures[J]. *Physical Review Letters*, 2008, 100(25): 256803.

[6] GAN Q Q, DING Y J, BARTOLI F J. “Rainbow” trapping and releasing at telecommunication wavelengths[J]. *Physical Review Letters*, 2009, 102(5): 056801.

[7] MAIER S A, ANDREWS S R, MARTÍN-MORENO L, *et al*.. Terahertz surface plasmon-polariton propagation and focusing on periodically corrugated metal wires[J]. *Physical Review Letters*, 2006, 97(17): 176805.

[8] ZHANG Y, XU Y H, TIAN CH X, *et al*.. Terahertz spoof surface-plasmon-polariton subwavelength waveguide[J]. *Photonics Research*, 2018, 6(1): 18-23.

[9] XU W D, XIE L J, YING Y B. Mechanisms and applications of terahertz metamaterial sensing: a review[J]. *Nanoscale*, 2017, 9(37): 13864-13878.

[10] SHALTOUT A M, SHALAEV V M, BRONGERSMA M L. Spatiotemporal light control with active metasurfaces[J]. *Science*, 2019, 364(6441): eaat3100.

[11] ZHANG X Y, LI Q, LIU F F, *et al*.. Controlling angular dispersions in optical metasurfaces[J]. *Light*: *Science* & *Applications*, 2020, 9(1): 76.

[12] SUN SH L, HE Q, XIAO SH Y, *et al*.. Gradient-index meta-surfaces as a bridge linking propagating waves and surface waves[J]. *Nature Materials*, 2012, 11(5): 426-431.

[13] NI X J, EMANI N K, KILDISHEV A V, *et al*.. Broadband light bending with plasmonic nanoantennas[J]. *Science*, 2012, 335(6067): 427.

[14] HUANG L L, CHEN X ZH, MÜHLENBERND H, *et al*.. Dispersionless phase discontinuities for controlling light propagation[J]. *Nano Letters*, 2012, 12(11): 5750-5755.

[15] GENEVET P, CAPASSO F, AIETA F, *et al*.. Recent advances in planar optics: from plasmonic to dielectric metasurfaces[J]. *Optica*, 2017, 4(1): 139-152.

[16] MUELLER J P B, RUBIN N A, DEVLIN R C, *et al*.. Metasurface polarization optics: independent phase control of arbitrary orthogonal states of polarization[J]. *Physical Review Letters*, 2017, 118(11): 113901.

[17] DECKER M, STAUDE I, FALKNER M, *et al*.. High-efficiency dielectric Huygens' surfaces[J]. *Advanced Optical Materials*, 2015, 3(6): 813-820.

[18] LIU L X, ZHANG X Q, KENNEY M, *et al*.. Broadband metasurfaces with simultaneous control of phase and amplitude[J]. *Advanced Materials*, 2014, 26(29): 5031-5036.

[19] GAO Y SH, FAN Y B, WANG Y J, *et al*.. Nonlinear holographic all-dielectric metasurfaces[J]. *Nano Letters*, 2018, 18(12): 8054-8061.

[20] LI G X, CHEN SH M, PHOLCHAI N, *et al*.. Continuous control of the nonlinearity phase for harmonic generations[J]. *Nature Materials*, 2015, 14(6): 607-612.

[21] KOSHELEV K, TANG Y T, LI K F, *et al*.. Nonlinear metasurfaces governed by bound states in the continuum[J]. *ACS Photonics*, 2019, 6(7): 1639-1644.

[22] KRASNOK A, TYMCHENKO M, ALÙ A. Nonlinear metasurfaces: a paradigm shift in nonlinear optics[J]. *Materials Today*, 2018, 21(1): 8-21.

[23] YE W M, ZEUNER F, LI X, *et al*.. Spin and wavelength multiplexed nonlinear metasurface holography[J]. *Nature Communications*, 2016, 7: 11930.

[24] CHEN X ZH, HUANG L L, MÜHLENBERND H, *et al*.. Dual-polarity plasmonic metalens for visible light[J]. *Nature Communications*, 2012, 3: 1198.

[25] KHORASANINEJAD M, CHEN W T, DEVLIN R C, *et al*.. Metalenses at visible wavelengths: diffraction-limited focusing and subwavelength resolution imaging[J]. *Science*, 2016, 352(6290): 1190-1194.

[26] WANG SH M, WU P C, SU V C, *et al*.. A broadband achromatic metalens in the visible[J]. *Nature Nanotechnology*, 2018, 13(3): 227-232.

[27] HUANG L L, CHEN X ZH, MÜHLENBERND H, *et al*.. Three-dimensional optical holography using a plasmonic metasurface[J]. *Nature Communications*, 2013, 4: 2808.

[28] LI L L, CUI T J, JI W, *et al*.. Electromagnetic reprogrammable coding-metasurface holograms[J]. *Nature Communications*, 2017, 8(1): 197.

[29] ZHENG G X, MÜHLENBERND H, KENNEY M, *et al*.. Metasurface holograms reaching 80% efficiency[J]. *Nature Nanotechnology*, 2015, 10(4): 308-312.

[30] TITTL A, LEITIS A, LIU M K, *et al*.. Imaging-based molecular barcoding with pixelated dielectric metasurfaces[J]. *Science*, 2018, 360(6393): 1105-1109.

[31] STAUDE I, SCHILLING J. Metamaterial-inspired silicon nanophotonics[J]. *Nature Photonics*, 2017, 11(5): 274-284.

[32] ZHANG SH, FAN W J, MINHAS B K, *et al*.. Midinfrared resonant magnetic nanostructures exhibiting a negative permeability[J]. *Physical Review Letters*, 2005, 94(3): 037402.

[33] YAO J, LIU ZH W, LIU Y M, *et al*.. Optical negative refraction in bulk metamaterials of nanowires[J]. *Science*, 2008, 321(5891): 930.

[34] HENTSCHEL M, SCHÄFERLING M, DUAN X Y, *et al*.. Chiral plasmonics[J]. *Science Advances*, 2017, 3(5): e1602735.

[35] ZHANG SH, PARK Y S, LI J, *et al*.. Negative refractive index in chiral metamaterials[J]. *Physical Review Letters*, 2009, 102(2): 023901.

[36] KANG L, WANG CH Y, GUO X X, *et al*.. Nonlinear chiral meta-mirrors: enabling technology for ultrafast switching of light polarization[J]. *Nano Letters*, 2020, 20(3): 2047-2055.

[37] ASADCHY V S, DÍAZ-RUBIO A, TRETYAKOV S A. Bianisotropic metasurfaces: physics and applications[J]. *Nanophotonics*, 2018, 7(6): 1069-1094.
[38] DORRAH A H, ELEFTHERIADES G V. Bianisotropic Huygens' metasurface pairs for nonlocal power-conserving wave transformations[J]. *IEEE Antennas and Wireless Propagation Letters*, 2018, 17(10): 1788-1792.
[39] YAZDI M, ALBOOYEH M, ALAEE R. A bianisotropic metasurface with resonant asymmetric absorption[J]. *IEEE Transactions on Antennas and Propagation*, 2015, 63(7): 3004-3015.
[40] WANG X CH, DÍAZ-RUBIO A, ASADCHY V S, *et al*.. Extreme asymmetry in metasurfaces via evanescent fields engineering: angular-asymmetric absorption[J]. *Physical Review Letters*, 2018, 121(25): 256802.
[41] GUO Q H, GAO W L, CHEN J, *et al*.. Line degeneracy and strong spin-orbit coupling of light with bulk bianisotropic metamaterials[J]. *Physical Review Letters*, 2015, 115(6): 067402.
[42] KHANIKAEV A B, MOUSAVI S H, TSE W K, *et al*.. Photonic topological insulators[J]. *Nature Materials*, 2013, 12(3): 233-239.
[43] YANG B, GUO Q H, TREMAIN B, *et al*.. Ideal Weyl points and helicoid surface states in artificial photonic crystal structures[J]. *Science*, 2018, 359(6379): 1013-1016.
[44] JIA H W, ZHANG R X, GAO W L, *et al*.. Observation of chiral zero mode in inhomogeneous three-dimensional Weyl metamaterials[J]. *Science*, 2019, 363(6423): 148-151.
[45] YANG B, BI Y G, ZHANG R X, *et al*.. Momentum space toroidal moment in a photonic metamaterial[J]. *Nature Communications*, 2021, 12(1): 1784.
[46] PENG L, DUAN L F, WANG K W, *et al*.. Transverse photon spin of bulk electromagnetic waves in bianisotropic media[J]. *Nature Photonics*, 2019, 13(12): 878-882.
[47] XIA L B, YANG B, GUO Q H, *et al*.. Simultaneous TE and TM designer surface plasmon supported by bianisotropic metamaterials with positive permittivity and permeability[J]. *Nanophotonics*, 2019, 8(8): 1357-1362.

Author Biographics:

YOU Ou-bo (1989 —), male, born in Quzhou, Zhejiang Province. He received his bachelor and Ph.D. degrees in Department of Precision Instrument, Tsinghua University in 2017. Currently, he is a postdoc fellow in the Department of Physics at the University of Hong Kong. His main research interests include metamaterials and nanophotonics. E-mail: yououbo@hku.hk

ZHANG Shuang (1975—), male, born in Dalian, Liaoning province. Currently, he is a chair professor in the Department of Physics and the Department of Electrical & Electronic Engineering at the University of Hong Kong. He received his Ph.D. degree in Electrical Engineering from the University of New Mexico in 2005, and elected as OSA member in 2016. He has made many important achievements in field of metamaterial. E-mail: shuzhang@hku.hk

XIANG Yuan-jiang (1978 —), male, born in Taizhou, Zhejiang Province. He received the M.S. degree in physics and microelectronics sciences and the Ph.D. degree in computer application technology from Hunan University, China, in 2006 and 2011, respectively. He is currently a Professor with Hunan University. His main research interest includes the transmission and control of light and electromagnetic waves. E-mail: xiangyuanjiang@126.com